APPLICATIONS OF AN IMPLICIT-COMPOSED INTEGRATION SCHEME TO NON-LINEAR DYNAMIC ANALYSIS

William Taylor Matias Silva, taylor@unb.br
Luciano Mendes Bezerra, lmbz@unb.br
University of Brasilia

Abstract. *In this work we focus on a simple implicit time integration scheme for transient response solution of structures when large deformations and long time durations are considered. Our aim is to have a practical method of implicit time integration for analyses in which the widely used Newmark time integration procedure is not conserving energy and momentum, and is unstable. The method of time integration discussed in this paper is performing well and is a good candidate for practical analyses.*

Keywords: *Nonlinear dynamics, implicit time integration, conservation of momentum and energy*

1. INTRODUCTION

In the last four decades, the computational mechanics community has accomplished many researches trying to propose effective methods for non-linear dynamic analysis in the framework of the finite element method. For fast transient analyses, for example impact problems, explicit methods are largely used. However, these methods are conditionally stables and ask for very small time steps to get reasonable solutions. For transient analyses of long duration, as in vibration problems of structural systems, the implicit methods are more effective. The first implicit integration procedures used are Houbolt, Newmark and Wilson-θ, Bathe (1996). Among these methods, the Newmark method and its particular case, the trapezoidal rule, became very popular and effective for linear dynamic analysis of practical problems. The trapezoidal rule scheme is the most effective because it is a second order method and uses simple time steping. However, in non-linear dynamic analysis, the trapezoidal rule becomes considerable unstable. Such instability is due to the pathological growth of the total potential energy and the angular momentum. The trapezoidal rule integration scheme does not guarantee the conservation of the momentum-energy along the time. To overcome this inconvenient characteristic, many implicit algorithms were additionally proposed based in the following ideas, Kuhl and Crisfield (1999):

1. Introduction of numeric dissipation, Chung and Hulbert (1993);

2. Conservation of the momentum-energy throughout the use of Lagrange multipliers, Kuhl and Ramm (1996);

3. Imposition, in the algorithm, of the momentum-energy conservation, Simo and Tarnow (1992).

The present work extends the application of the trapezoidal rule scheme to non-linear dynamic analyses. To keep the conservation of the momentum-energy, the trapezoidal rule scheme is combined to the descent finite difference scheme at three different points within an arbitrary time interval. It is noted that both schemes are very much employed in numerical procedures to solve ordinary differential equations, Collatz (1966). Bank et al (1985) use the combination of both schemes to solve first order ordinary differential equations that simulate the behavior of electric circuits or computer processors for super-computing. Recently, Bathe (2007), Bathe and Baig (2005) utilized such mixed algorithm schemes to get solutions of second order differential equations describing the dynamic equilibrium of structural systems. Those authors obtained transient responses for plates and beam discritizing them with solid 2D finite elements. The plates and beams studied by such authors were under large translations and rotations due to rigid-body motions. In the next section, the coupling of these two schemes (trapezoidal rule and descent finite difference) is explained in details.

2. THE IMPLICIT-COMPOSED ALGORITHM

The equation of motion of a deformable body discretized by the finite element method may be expressed by the following matricial equation

$$\mathbf{M}\ddot{\mathbf{u}} + \mathbf{C}\dot{\mathbf{u}} + \mathbf{f}(\mathbf{u}, t) = \mathbf{p}(t) \tag{1}$$

where $\mathbf{M}$ is the mass matrix, $\mathbf{C}$ is the damping matrix, $\mathbf{f}$ is the vector of internal forces and $\mathbf{p}(t)$ the vector of external forces. Moreover, $\ddot{\mathbf{u}}$, $\dot{\mathbf{u}}$ and $\mathbf{u}$ are, respectively, the vectors of displacements, velocities and accelerations. We assume here that $\mathbf{M}$ and $\mathbf{C}$ are constant matrices and we also observe that equation (1) is a non-linear equation because the internal forces vector is a function of the displacement $\mathbf{u}$. In general, time integration algorithms to solve equation (1) are formulated throughout the finite difference schemes and such schemes show some sort of numerical dissipation. This

dissipation property may be good in getting better numerical stabilization of such integration schemes. The implicit-composed scheme divides any time interval in two sub-intervals. In the first sub-interval, the trapezoidal rule is applied while in the second sub-interval we make use of the descent finite difference scheme with three points. As the application of the algorithm aims non-linear analyses, it is necessary to establish an incremental-iterative strategy to get the final solution. In this work, the Newton-Raphson method, in the iterative phase, is used to dissipate the residual forces or the vector of the unbalanced forces. Therefore, the kinematics equation may be written as a function of the displacements, and later on, such equation is developed in Taylor's series up to the first order terms.

2.1 First sub-interval

At first, it is assumed that the solution of the kinematics equation is known at time t_n and we wish to get a solution at time t_{n+1}, such that, $t_{n+1} = t_n + \Delta t$. Consider $t_{n+\gamma} = t_n + \gamma \Delta t$, a time instance between t_n and t_{n+1}, with $\gamma \in (0, 1)$. Applying now the trapezoidal rule over the time interval, $\gamma \Delta t$, one gets velocities and displacements for the time $t_{n+\gamma}$, by means of the following finite difference equations, respectively

$$\dot{\mathbf{u}}_{n+\gamma} = \dot{\mathbf{u}}_n + \frac{\ddot{\mathbf{u}}_n + \ddot{\mathbf{u}}_{n+\gamma}}{2} \gamma \Delta t \tag{2}$$

$$\mathbf{u}_{n+\gamma} = \mathbf{u}_n + \frac{\dot{\mathbf{u}}_n + \dot{\mathbf{u}}_{n+\gamma}}{2} \gamma \Delta t \tag{3}$$

Substituting equation (2) into equation (3), one obtains

$$\mathbf{u}_{n+\gamma} = \mathbf{u}^*_{n+\gamma} + \frac{\gamma^2 \Delta t^2}{4} \ddot{\mathbf{u}}_{n+\gamma} \tag{4}$$

with

$$\mathbf{u}^*_{n+\gamma} = \mathbf{u}_n + \gamma \Delta t \dot{\mathbf{u}}_n + \frac{\gamma^2 \Delta t^2}{4} \ddot{\mathbf{u}}_n \tag{5}$$

On the other hand, equation (2) may be rewritten as

$$\dot{\mathbf{u}}_{n+\gamma} = \dot{\mathbf{u}}^*_{n+\gamma} + \frac{\gamma \Delta t}{2} \ddot{\mathbf{u}}_{n+\gamma} \tag{6}$$

with

$$\dot{\mathbf{u}}^*_{n+\gamma} = \dot{\mathbf{u}}_n + \frac{\gamma \Delta t}{2} \ddot{\mathbf{u}}_n \tag{7}$$

Therefore, the accelerations and velocities may be obtained, using equations (4) and (6) as

$$\ddot{\mathbf{u}}_{n+\gamma} = \frac{4}{\gamma^2 \Delta t^2} (\mathbf{u}_{n+\gamma} - \mathbf{u}^*_{n+\gamma}) \tag{8}$$

$$\dot{\mathbf{u}}_{n+\gamma} = \dot{\mathbf{u}}^*_{n+\gamma} + \frac{2}{\gamma \Delta t} (\mathbf{u}_{n+\gamma} - \mathbf{u}^*_{n+\gamma}) \tag{9}$$

The kinematics equation (1) at time $t + \gamma \Delta t$ may be rewritten as

$$\mathbf{M} \ddot{\mathbf{u}}_{n+\gamma} + \mathbf{C} \dot{\mathbf{u}}_{n+\gamma} + \mathbf{f}_{n+\gamma}(\mathbf{u}_{n+\gamma}) = \mathbf{p}_{n+\gamma} \tag{10}$$

Substituting equations (8) and (9) into equation (10), expanding the resulting equation (10) into a Taylor's series as a function of the displacements $\mathbf{u}_{n+\gamma}$, and considering only the first order terms, one gets

$$\left(\mathbf{K}_{n+\gamma}^i + \frac{4}{\gamma^2 \Delta t^2}\mathbf{M} + \frac{2}{\gamma \Delta t}\mathbf{C}\right)\Delta\mathbf{u}_{n+\gamma}^{i+1} =$$

$$\mathbf{p}_{n+\gamma} - \left\{\mathbf{f}_{n+\gamma}^i + \mathbf{M}\left[\frac{4}{\gamma^2 \Delta t^2}(\mathbf{u}_{n+\gamma}^i - \mathbf{u}_{n+\gamma}^*)\right] + \mathbf{C}\left[\dot{\mathbf{u}}_{n+\gamma}^* + \frac{2}{\gamma \Delta t}(\mathbf{u}_{n+\gamma}^i - \mathbf{u}_{n+\gamma}^*)\right]\right\} \tag{11}$$

with $\mathbf{u}_{n+\gamma}^{i+1} = \mathbf{u}_{n+\gamma}^i + \Delta\mathbf{u}_{n+\gamma}^{i+1}$, and $\mathbf{K}_{n+\gamma}^i = \frac{\partial \mathbf{f}_{n+\gamma}^i}{\partial \mathbf{u}_{n+\gamma}^i}$, being the consistent tangent stiffness matrix at the configuration corresponding to the displacements $\mathbf{u}_{n+\gamma}^i$. Once the displacements are determined, the accelerations and velocities may be obtained by means of equations (8) and (9), respectively. For more details, see the incremental-iterative flow diagram represented in Figure 1.
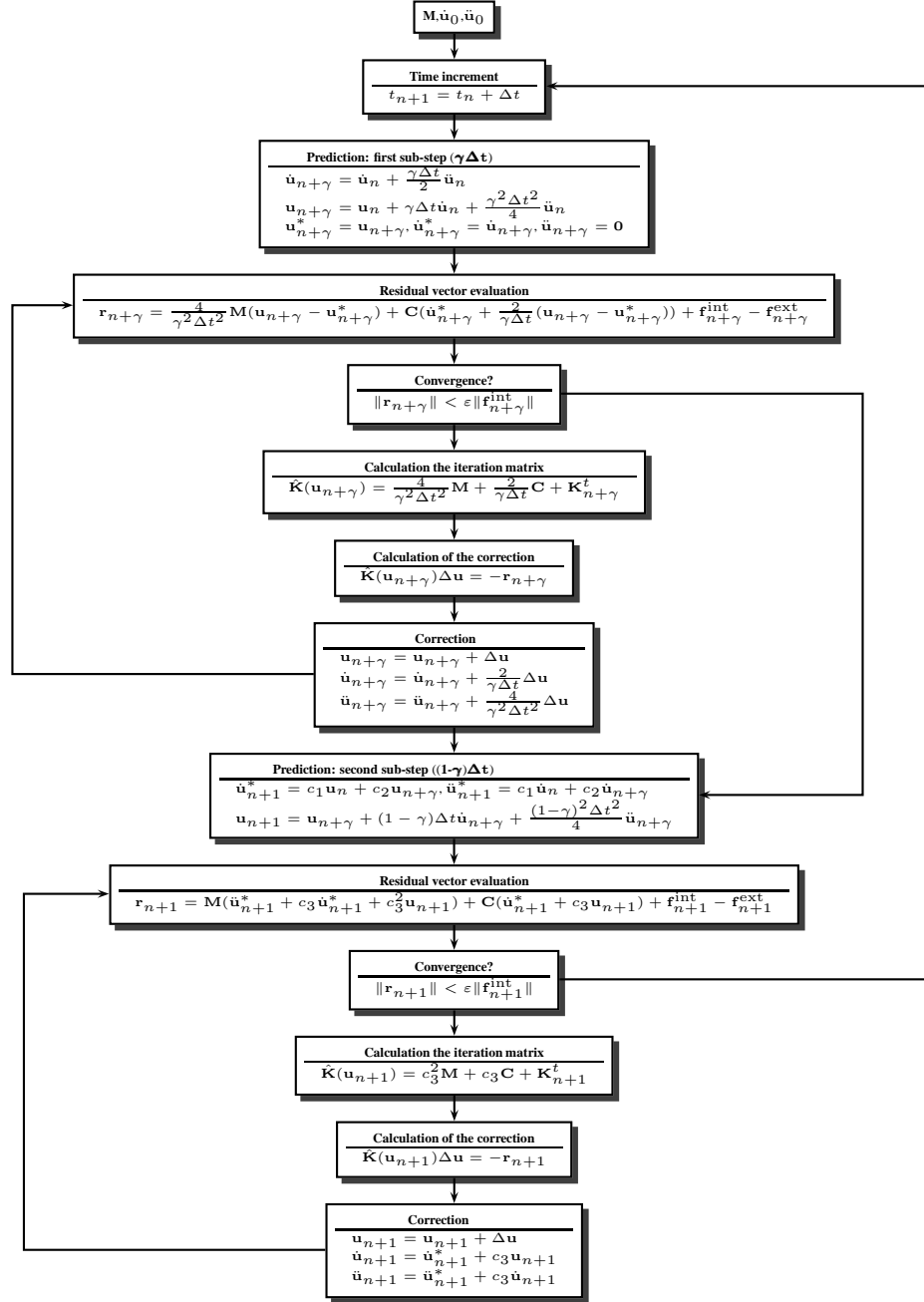
Figure 1. Incremental-iterative scheme of the implicit-composed algorithm

2.2 Second sub-interval

Let the derivative of a function f at time $t + \Delta t$ be written in terms of the derivatives of the function values at times t, $t + \gamma \Delta t$ and $t + \Delta t$ as Collatz (1966)

$$\dot{f}_{n+1} = c_1 f_n + c_1 f_{n+\gamma} + c_3 f_{n+1} \tag{12}$$

where

$$
\begin{aligned}
c_1 &= \frac{(1-\gamma)}{\gamma \Delta t} \\
c_2 &= \frac{-1}{(1-\gamma)\gamma \Delta t} \\
c_3 &= \frac{(2-\gamma)}{(1-\gamma)\Delta t}
\end{aligned}
\tag{13}
$$

Thus, the velocities as functions of the displacements and the accelerations as functions of velocities at time $t + \Delta t$ may be determined by the following equations

$$\dot{\mathbf{u}}_{n+1} = c_1 \mathbf{u}_n + c_2 \mathbf{u}_{n+\gamma} + c_3 \mathbf{u}_{n+1} \tag{14}$$

$$\ddot{\mathbf{u}}_{n+1} = c_1 \dot{\mathbf{u}}_n + c_2 \dot{\mathbf{u}}_{n+\gamma} + c_3 \dot{\mathbf{u}}_{n+1} \tag{15}$$

These equations may be rewritten as

$$\dot{\mathbf{u}}_{n+1} = \dot{\mathbf{u}}^*_{n+1} + c_3 \mathbf{u}_{n+1} \tag{16}$$

$$\ddot{\mathbf{u}}_{n+1} = \ddot{\mathbf{u}}^*_{n+1} + c_3 \dot{\mathbf{u}}_{n+1} \tag{17}$$

with

$$\dot{\mathbf{u}}^*_{n+1} = c_1 \mathbf{u}_n + c_2 \mathbf{u}_{n+\gamma} \tag{18}$$

$$\ddot{\mathbf{u}}^*_{n+1} = c_1 \dot{\mathbf{u}}_n + c_2 \dot{\mathbf{u}}_{n+\gamma} \tag{19}$$

Substituting equation (16) into equation (17), one gets

$$\ddot{\mathbf{u}}_{n+1} = \ddot{\mathbf{u}}^*_{n+1} + c_3 \dot{\mathbf{u}}^*_{n+1} + c_3^2 \mathbf{u}_{n+1} \tag{20}$$

The kinematics equation (1) at time $t + \Delta t$ may be written as

$$\mathbf{M}\ddot{\mathbf{u}}_{n+1} + \mathbf{C}\dot{\mathbf{u}}_{n+1} + \mathbf{f}_{n+1}(\mathbf{u}_{n+1}) = \mathbf{p}_{n+1} \tag{21}$$

Substituting equations (16) and (20) into equation (21), expanding the resulting equation into a Taylor's series as a function of the displacements $\mathbf{u}_{n+1}$, and up to the first order terms, we obtain

$$
\begin{aligned}
\left(\mathbf{K}^i_{n+1} + c_3^2 \mathbf{M} + c_3 \mathbf{C}\right) \Delta \mathbf{u}^{i+1}_{n+1} = \\
\mathbf{p}_{n+1} - \left\{\mathbf{f}^i_{n+1} + \mathbf{M}(\ddot{\mathbf{u}}^*_{n+1} + c_3 \dot{\mathbf{u}}^*_{n+1} + c_3^2 \mathbf{u}_{n+1}) + \mathbf{C}(\dot{\mathbf{u}}^*_{n+1} + c_3 \mathbf{u}_{n+1})\right\}
\end{aligned}
\tag{22}
$$

with $\mathbf{u}^{i+1}_{n+1} = \mathbf{u}^i_{n+1} + \Delta \mathbf{u}^{i+1}_{n+1}$. The tangent stiffness matrix $\mathbf{K}^i_{n+1} = \frac{\partial \mathbf{f}^i_{n+1}}{\partial \mathbf{u}^i_{n+1}}$ and the internal forces vector $\mathbf{f}^i_{n+1}$, are obtained in a consistent way at the configuration corresponding to the displacements $\mathbf{u}^i_{n+1}$. Once the displacements are determined, the accelerations and velocities may be calculated according to equations (16) and (17), respectively. For more details, examine the incremental-iterative flow diagram represented in Figure 1.

3. NUMERICAL EXAMPLES

In the following examples, one finite element in 2D space representing a bi-articulated bar is used. The internal forces vector and the stiffness matrix of such finite element are obtained from a Total Lagrangean Formulation. For more details of such formulation, read the references Matias (2004,2005). The mass matrix considered in the following examples consider the mass of the bar element as concentrated at the two end nodes. To find the transient response, the incremental-iterative scheme illustrated in Figure 1 is used with a numerical tolerance on the norm of the residual force vector taken as 10^{-5}. We remind that the objective of the present article is to exam the performance of the implicit-composed algorithm described in section 2 when larger time stepping is adopted for long time intervals. With this in mind, it is important to analyze whether the algorithm presents the following undesirable aspects: (1) excessive errors in the period and in the amplitud of the transient response; (2) strong growth of the total potential energy and of the angular momentum; (3) strong decline of the total potential energy and of the angular momentum; and (4) lack of convergence during the iterative process.

3.1 Rigid pendulum
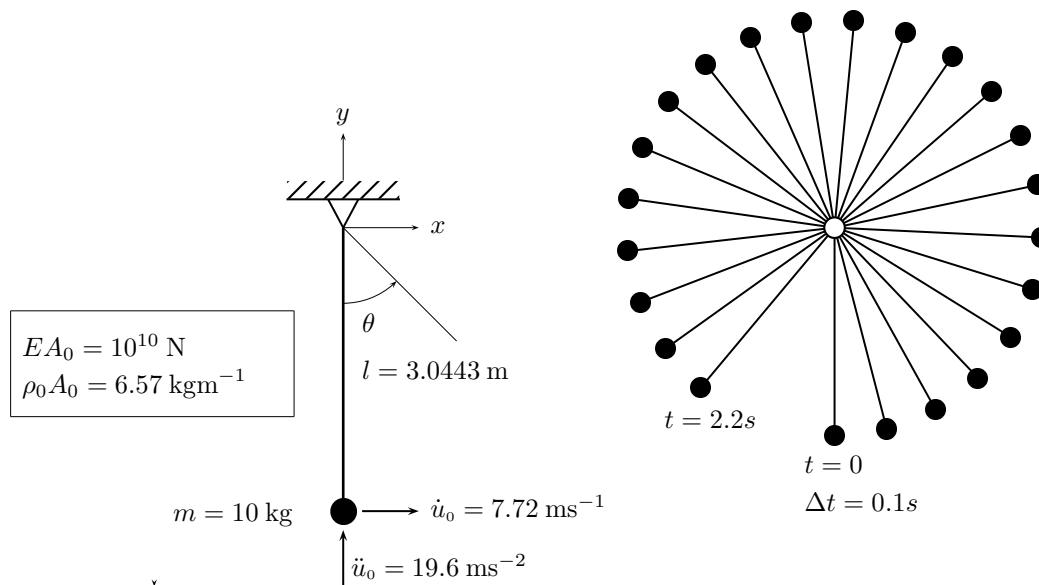
Figure 2. Rigid pendulum. Data and initial conditions

Among other authors, Bathe (2006), Crisfield and Shi (1994), and Kuhl and Crisfield (1999), analyzed this example. The geometrical and physical characteristics of the rigid pendulum, the initial conditions, the boundary conditions and other data of the problem are in Figure 2. The rigid pendulum was discretized with one bi-articulated finite element bar in 2D space, having two degrees of freedom restrained and two degrees of freedom released. The rigid pendulum has an axial stiffness of $EA = 10^{10}$ N. Initial velocity and acceleration are considered. No gravitational force is considered, and, therefore, no external force is applied at the free end node of the pendulum. Therefore, the total potential energy and the angular momentum are kept constants. Moreover, the total potential energy is easily found to be $\pi_0 = \frac{1}{2}m\dot{u}_0^2 = 298$ Nm, and the angular momentum $\mathcal{H}_0 = lm\dot{u}_0 = 235$ kgm^{2}s^{-1}. The period of this pendulum is given by $T = \pi\sqrt{\frac{2l}{g}} = 2.47$ s, which corresponds to an angle of $360°$, that is; 1 cycle or a complete turn around in 2.47s. We take on three time steps: $\Delta t = 0.01$ s, $\Delta t = 0.1$ s e $\Delta t = 0.6$ s, corresponding to the following ratios to the period $\frac{\Delta t}{T}$ of 0.004, 0.04 e 0.24; and also to the following angles: $1.45°$, $14.5°$ e $87.3°$, respectively. These angles represent, respectively, small, moderate, and large rotations. The transient analysis is carried out for a total time duration of 50 s which means 20 cycles. Figure 3a shows the mass trajectories for the three different time steps adopted; observe the coincidence between the trajectories. Examining Figure 3b, for $\Delta t = 0.01$ s, the numerical dissipation detected is negligible either for the total potential energy as well as for the angular momentum. However, for $\Delta t = 0.1$ s, the numerical dissipations along the time is noticeable. On the other hand, for $\Delta t = 0.6$ s, an excessive numerical dissipation of the total potential energy and the angular momentum is observed. Consequently, errors of great magnitude in the period and in the transient response may be observed in Figures 3c, 3d and 3e, respectively, for displacements, velocities and accelerations. Errors in the periods of the displacements may be noticed for time steps of $\Delta t = 0.1$ s and $\Delta t = 0.6$ s from the seventh cycle on. Those errors have a tendency to increase along the next cycles. With respect to velocity and acceleration, it may be observed that there
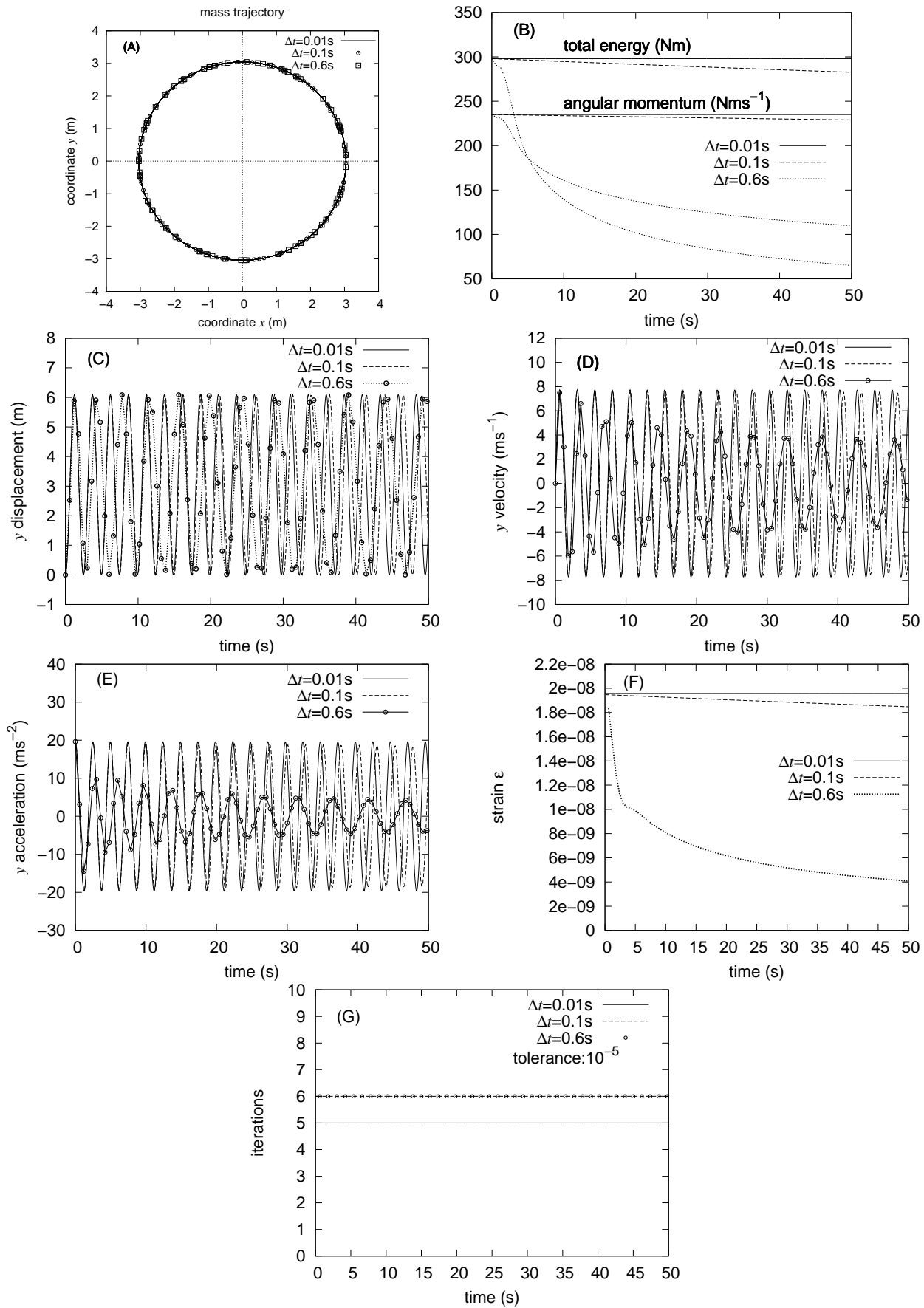
Figure 3. Rigid pendulum. Solution with the implicit-composed algorithm.

are errors in the period and in the amplitud for $\Delta t = 0.1$ s, and errors increase from the seventh cycle on. For $\Delta t = 0.6$ s, the errors are meaningful and the transient responses are short of precision to represent the physical model under analysis. In Figure 5, the magnitude of deformation do not exceed $\epsilon \leq 2 \times 10^{-8}$ due to the hypothesis of rigid-body motion. Considering the different time steps used to solve this problem, Figure-3g shows the evolution of the number of iterations along the time necessary to get convergence in the solution. It is important to point out that such figure deals with the sum of the iterations corresponding to the two sub-intervals, that is; $[t_n; t_{n+\gamma}]$ and $[t_{n+\gamma}; t_{n+1}]$. Finally, it is worth mentioning that the algorithm presented here showed numerical stability even when large time step is used, for example, $\Delta t = 0.6$ s. No strong growth was observed for the momentum-energy of the system as can be seen in Figure 3b.

3.2 System with 5 spheres connected with massless and rigid rods

Crisfield and Shi (1994) analyzed this example. Figure 4a shows a chain of pinned bars (truss element) that is free to fly in the absence of gravity. Initially, the bars lie horizontally with no velocity in the x direction but a linear distribution of vertical velocity. Under such conditions, the chain should remain straight moving downwards and rotating at the same time. The system has 5 spherical masses connected with weightless rigid rods. The geometrical and physical characteristics of the five connected spheres, the initial conditions, the boundary conditions, and other applicable data are summarized in Figure 4a. The initial conditions of the system are: (a) an angular velocity of $\omega_0 = \dot{\theta}_0 = 1 \, \mathrm{rads}^{-1}$ around the axis with the pole B (node 5) parallel to the z-axis which is equivalent a linear distribution of vertical velocity, and (b) a zero angular acceleration $\alpha_0 = \ddot{\theta}_0 = 0$. This system were discretized with four finite elements, bi-articulated bar elements in the 2D space. The finite element model has five nodes making a total of 10 degrees of freedom. There are no constraint nodes. Gravitational forces are not considered and, therefore, the total potential energy and the angular momentum are kept constant along the time considered for the analysis of this problem, $t = 50$ s. Due to the initial and boundary conditions, the system goes downwards in the vertical direction, y-axis, and rotates around an axis parallel to the z-axis. The center of mass of the system is in the z-axis. Therefore, the system of five masses is subjected to large translations and rotations in the xy-plane. The total potential energy is given by the expression $\pi_0 = 22ml^2\omega_0^2 = 0.11 \times 10^8$ Ncm, and the angular momentum, with respect to pole B (node 5), is $\mathcal{H}_0 = 44ml^2\omega_0 = 22 \times 10^8 \, \mathrm{kgcm}^2\mathrm{s}^{-1}$. The components of the displacement, velocity and acceleration vectors of node 1 (pole A) may be obtained by the following expression:

$$
\begin{array}{ll}
u_{x_1} = 2l(1 - \cos\omega_0 t); & u_{y_1} = -2l(\omega_0 t + \sin\omega_0 t) \\
\dot{u}_{x_1} = 2l\omega_0\sin\omega_0 t; & \dot{u}_{y_1} = -2l\omega_0(1 + \cos\omega_0 t) \\
\ddot{u}_{x_1} = 2l\omega_0^2\cos\omega_0 t; & \ddot{u}_{y_1} = 2l\omega_0^2\sin\omega_0 t
\end{array}
$$

The period of this system is given by $T = \frac{2\pi}{\omega_0} = 6.28$ s, which corresponds to a turn around of $360°$ of the rigid system. Three time steps were used for this example; $\Delta t = 0.01$ s, $\Delta t = 0.1$ s e $\Delta t = 1$ s, which corresponds to the following ratios to the period $\frac{\Delta t}{T}$ of 0.0016, 0.016 e 0.16, and to the following angles $0.57°$, $5.73°$ e $57.3°$, respectively. These angles represent small, moderate, and large rotations, respectively. The transient analysis is carried out for a total time duration of 50 s or approximately 8 cycles. In Figure 4b, the plot of displacement vs. time is compared to the plot of the exact solution for the displacement of node 1 in the direction of x-axis. In such figure a coincidence between numerical results and exact solution may be observed for the time steps $\Delta t = 0.01$ s and $\Delta t = 0.1$ s. On the other hand, for time step $\Delta t = 1$ s, there are significant errors in the period and also errors of less extent for the amplitud of the transient response. Note that those errors increases in the next cycles. For node 1 and in the direction of the y-axis, the plot velocity vs. time is compared to the corresponding exact solution in Figure 4c. Again, there is an excellent agreement between the velocities of the exact solution and the velocities obtained using time steps $\Delta t = 0.01$ s and $\Delta t = 0.1$ s. However, for time step $\Delta t = 1$ s, significant errors in the period and in the transient response are observed. It is clear, from the figure, that these errors increase in the subsequent cycles. It is important to notice that the displacement, velocity, and acceleration obtained for a time step of $\Delta t = 1$ s are not adequate to represent the physical problem studied here. In Figure 4e, the magnitude of deformation do not exceed $\epsilon \leq 1.1 \times 10^{-6}$ due to the hypothesis of rigid-body motion. Figure 4f shows, for $\Delta t = 0.01$ s and $\Delta t = 0.1$ s, the numerical dissipation for the total potential energy and for the angular momentum detected are irrelevant. However, for $\Delta t = 1$ s, an excessive numerical dissipation of the total potential energy and the angular momentum exists and tends to increase along the time. Considering the different time steps $\Delta t = 0.01$ s, $\Delta t = 0.1$ s and $\Delta t = 1$ s to solve this problem, Figure 4g shows the number of iterations along the time necessary to get convergence in the solution. As a final point, it is remarkable that the algorithm shows numerical stability even for large time step, for example for $\Delta t = 0.1$ s. This can be seen in Figure 4f noticing that no excessive increase of momentum-energy of the system is observed.

3.3 Elastic pendulum

This example was analyzed by Bathe (2006), Kuhl and Crisfield (1999) among other researchers. The geometrical and physical characteristics of the elastic pendulum, the initial conditions, the boundary conditions and other data of the
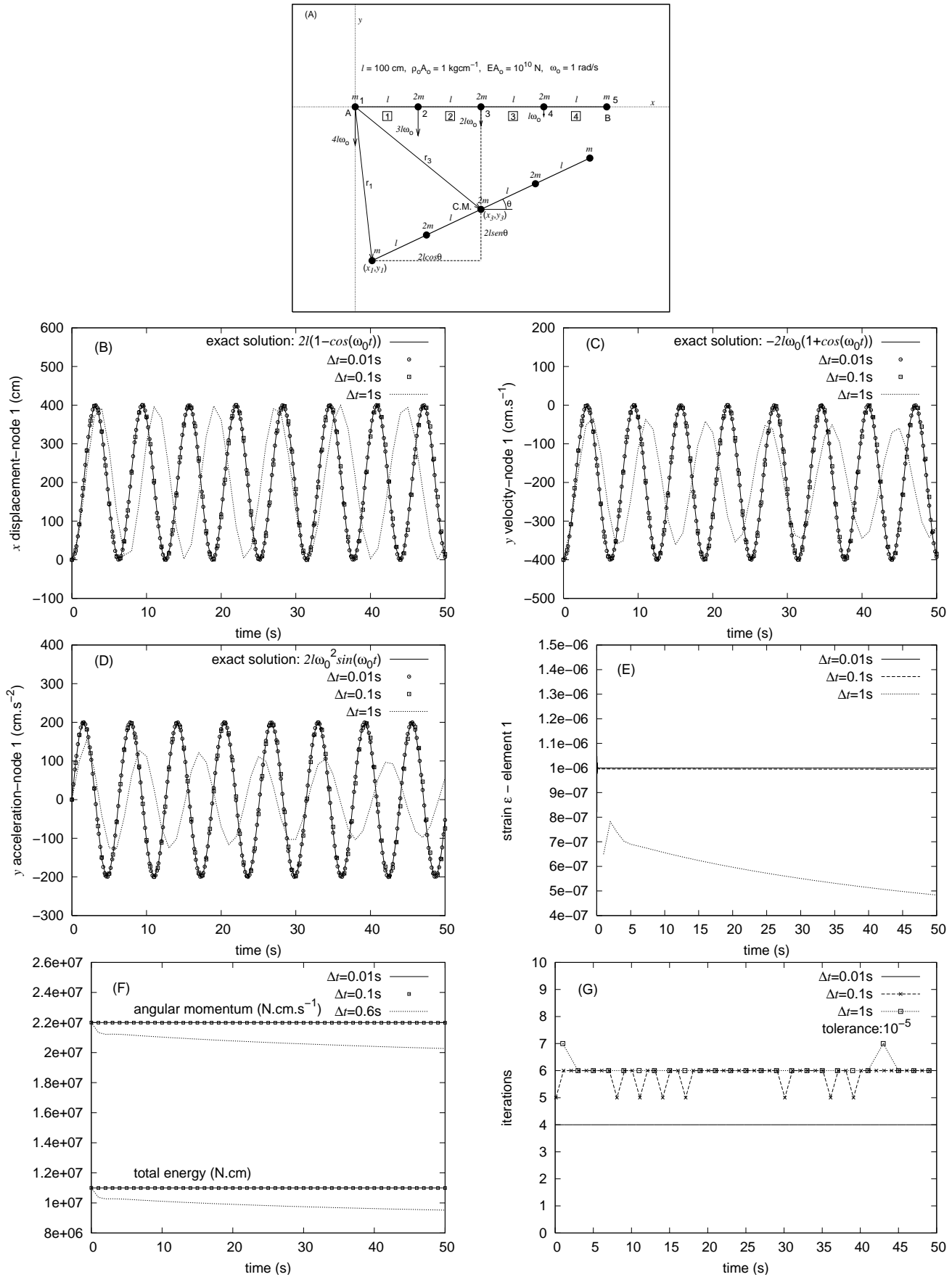
Figure 4. Four-bar-chain. Solution with the implicit-composed algorithm.

$$y$$

$$x$$

$$\theta$$

$$EA_0 = 10^4 \text{ N}$$
$$\rho_0 A_0 = 6.57 \text{ kgm}^{-1}$$

$$l = 3.0443 \text{ m}$$

$$m = 10 \text{ kg}$$

$$\dot{u}_o = 7.72 \text{ ms}^{-1}$$

$$\ddot{u}_o = 0 \text{ ms}^{-2}$$
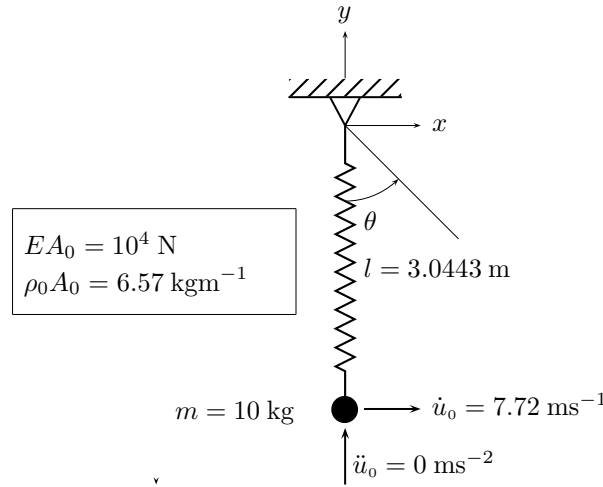
Figure 5. Elastic pendulum. Data and initial conditions

problem are in Figure 5. The pendulum was discretized with one bi-articuled 2D finite element bar which has two degrees of freedom restrained and two degrees of freedom released. An axial stiffness $EA = 10^4$ N is assumed. A non-zero initial velocity is considered. On the other, no gravitational force is assumed, and, therefore, no external force is applied at the free end node of the pendulum. Therefore, the total potential energy and the angular momentum are kept constants along the time. The potential energy is $\pi_0 = \frac{1}{2} m \dot{u}_0^2 = 298$ Nm and the angular momentum $\mathcal{H}_0 = lm\dot{u}_0 = 235 \text{ kgm}^2\text{s}^{-1}$. In this case, the period is given by $T = \pi\sqrt{\frac{2l}{g}} = 2.47$ s, which corresponds to an angle of $360°$, that is, 1 cycle or a complete turn around in 2.47 s. In adittion, in the case of an elastic pendulum, another oscillation frequency exists, a high axial frequency of $T = 0.28$ s. To capture this axial frequency two time steps are adopted: $\Delta t = 0.01$ s and $\Delta t = 0.05$ s corresponding to the following ratios to the period $\frac{\Delta t}{T}$ 0.036 and 0.18, respectively. Although, in this case, there are oscillations in high frequencies, no sudden growth is observed in the amplitud of the axial oscillations and in the energy-momentum of the oscillating system. These can be demonstrated in Figures 6b and 6f, respectively. Figure 6a shows the bar trajectories for the different time steps here considered. The coincidence of the trajectories is noticeable. Examining Figure 6b, for $\Delta t = 0.01$ s, the numerical dissipation detected is minimal either for the total potential energy as well as for the angular momentum. However, for $\Delta t = 0.05$ s, there are dissipations which tend to growth along the time. Figures 6c and 6d show the displacement and velocity of node 2 in the y-direction, respectively. In these figures, it can be observed that the transient responses are almost coincident for both time steps used. However, in the Figure 6e significant errors in the amplitud and in the acceleration period are observed. Furthermore, Figure 6f shows the axial oscillation, and exposes the significant erros in the period and in the amplitud due to the excessive numerical dissipation for $\Delta t = 0.05$ s. Attributable to this large Δt adopted for the algorithm it is impossible to detect a more precise response of the system under high frequency. Finally, Figure 6g presents the evolution to the solution convergence along the time of the number of iterations associated to each Δt adopted.

4. CONCLUSIONS

Concerning the performance of the implicit-composed algorithm applied to non-linear dynamic analysis, the following conclusions may be taken:

- The algorithm is easy to implement in a computer program;

- The mathematical formulation of the algorithm is very simple;

- The algorithm is effective to deal with large translations and rotations due to rigid-body motions;

- The algorithm presents an undesirable and excessive numerical dissipation for time steps Δt with ratios to the period $\frac{\Delta t}{T} > 0.1$;

- The computational cost of the algorithm is twice greater than the computational cost of the trapezoidal rule due to two iterative cycles needed in each time step;

- The algorithm preserves the momentum-energy without the need of Lagrange multipliers or without any imposition in the algorithm;
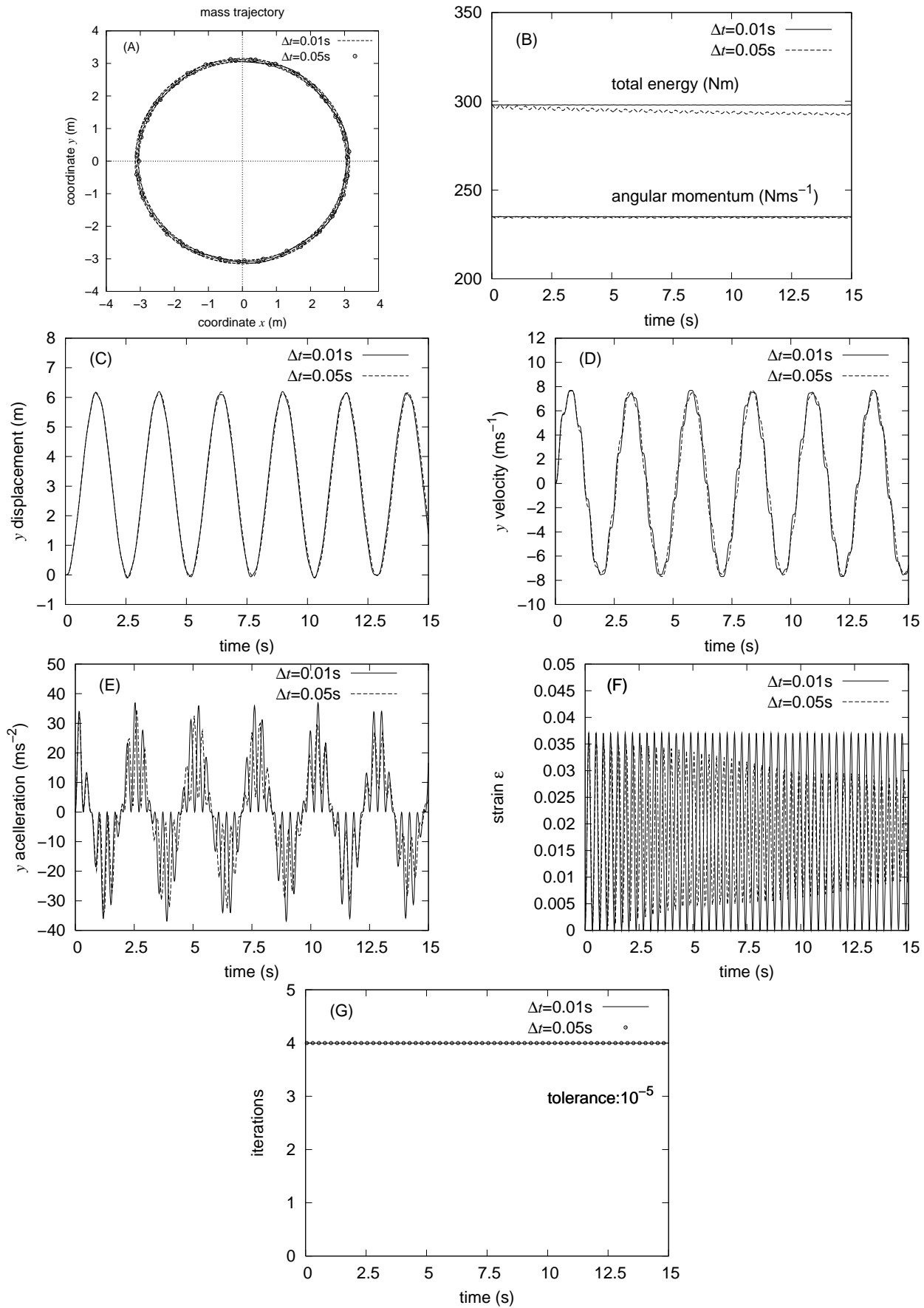
Figure 6. Elastic pendulum. Solution with the implicit-composed algorithm.

- The algorithm allows the user to work with symmetric matrices.

Finally, it is important to remind the need to study the implicit-composed scheme presented here from the mathematical point of view. With such study, the excessive numerical dissipation may be better understood and minimized. In the opinion of the authors, the numerical dissipation is the major drawback of the present scheme for its application in the numerical solution of practical engineering problems.

5. REFERENCES

Bank, R.E., Coughran Jr W.M., Fichtner W., Grosse, E.H., Rose, D.J. and Smith, R.K., 1985, Transient simulations of silicon devices and circuits. IEEE Trans CAD; CAD-4(4), 436–451.

Bathe, K.J., 1996, Finite element procedures, Prentice Hall.

Bathe, K.J., 2006, Conserving energy and momentum in nonlinear dynamics: A simple implicit time integration scheme, Computers & Structures, 85, 437–445.

Bathe, K.J. and Baig, M.M.I., 2005, On a composite implicit time integration procedure for nonlinear dynamics, Computers & Structures, 83, 2513–2524.

Chung, J. and Hulbert, G.M., 1993, A time integration algorithm for structural dynamics with improved numerical dissipation: the generalized alpha-method, Journal of Applied Mechanics, Transactions of the ASME, 60, 371–375.

Collatz L., 1966, The numerical treatment of differential equations, third edition, New York, Springer-Verlag.

Crisfield, M.A. and Shi, J., 1994, A co-rotational element/time integration strategy for non-linear dynamics, International Journal for Numerical Methods in Engineering, 37, 1897–1913.

Kuhl, D. and Crisfield, M.A., 1999, Energy-conserving and decaying algorithms in non-linear structural dynamics, International Journal for Numerical Methods in Engineering, 45, 569–599.

Kuhl, D. and Ramm, E., 1996, Constraint energy momentum algorithm and its application to nonlinear structural dynamics, Computer Methods in Applied Mechanics and Engineering, 136, 293–315.

Matias, W.T., 2005, Aplicaciones de algoritmos que conservan la energía-momentum en dinámica no-lineal, Congreso de Métodos Numéricos en Ingeniería 2005, Granada, España.

Matias, W.T., 2004, Aplicaciones de algoritmos que conservan la energía-momentum en dinámica no-lineal. PI 259. Centro Internacional de Métodos Numéricos en Ingeniería - CIMNE/UPC, Barcelona, España.

Simo, J.C. and Tarnow, N., 1992, The discrete energy-momentum method. Conserving algorithms for nonlinear elastodynamics, Journal of Applied Mathematics and Physics, 43, 757–792.

6. Responsibility notice

The authors are the only responsible for the printed material included in this paper.